

Retraction

Retracted: Prediction and Risk Assessment of Extreme Weather Events Based on Gumbel Copula Function

Journal of Function Spaces

Received 3 October 2023; Accepted 3 October 2023; Published 4 October 2023

Copyright © 2023 Journal of Function Spaces. This is an open access article distributed under the Creative Commons Attribution License, which permits unrestricted use, distribution, and reproduction in any medium, provided the original work is properly cited.

This article has been retracted by Hindawi following an investigation undertaken by the publisher [1]. This investigation has uncovered evidence of one or more of the following indicators of systematic manipulation of the publication process:

- (1) Discrepancies in scope
- (2) Discrepancies in the description of the research reported
- (3) Discrepancies between the availability of data and the research described
- (4) Inappropriate citations
- (5) Incoherent, meaningless and/or irrelevant content included in the article
- (6) Peer-review manipulation

The presence of these indicators undermines our confidence in the integrity of the article's content and we cannot, therefore, vouch for its reliability. Please note that this notice is intended solely to alert readers that the content of this article is unreliable. We have not investigated whether authors were aware of or involved in the systematic manipulation of the publication process.

Wiley and Hindawi regrets that the usual quality checks did not identify these issues before publication and have since put additional measures in place to safeguard research integrity.

We wish to credit our own Research Integrity and Research Publishing teams and anonymous and named external researchers and research integrity experts for contributing to this investigation.

The corresponding author, as the representative of all authors, has been given the opportunity to register their agreement or disagreement to this retraction. We have kept a record of any response received.

References

- [1] P.-H. Yang, Y. Yu, F. Gu, M.-J. Qu, and J.-M. Zhu, "Prediction and Risk Assessment of Extreme Weather Events Based on Gumbel Copula Function," *Journal of Function Spaces*, vol. 2022, Article ID 1438373, 13 pages, 2022.

Research Article

Prediction and Risk Assessment of Extreme Weather Events Based on Gumbel Copula Function

Peng-Hui Yang ¹, Yao Yu ¹, Feng Gu ², Meng-Jie Qu ³, and Jia-Ming Zhu ¹

¹School of Statistics and Applied Mathematics, Anhui University of Finance and Economics, Bengbu 233030, China

²School of Finance, Anhui University of Finance and Economics, Bengbu 233030, China

³School of Accounting, Anhui University of Finance and Economics, Bengbu 233030, China

Correspondence should be addressed to Jia-Ming Zhu; zhujm1973@163.com

Received 1 May 2022; Accepted 28 June 2022; Published 21 July 2022

Academic Editor: Miaochoao Chen

Copyright © 2022 Peng-Hui Yang et al. This is an open access article distributed under the Creative Commons Attribution License, which permits unrestricted use, distribution, and reproduction in any medium, provided the original work is properly cited.

Damage caused by climate catastrophes is severe, especially for the 1-in-100-year events. This study is aimed at assessing the frequency and spatiotemporal regularity of extreme weather events. Based on the selected Gumbel copula function, a joint trivariate distribution of weather events is established. In this study, different univariate return periods and return periods of the joint trivariate distribution are calculated separately. Second, the Moran index is used to determine whether there is a spatial correlation between weather events. In this paper, the spatial and temporal patterns of weather events are determined based on a geographically weighted regression model. The suggestion of adding Bayesian information to the model measurements to improve the model accuracy is presented. Finally, a wavelet neural network model is constructed to predict the probability of extreme weather events throughout the Americas.

1. Introduction

Disasters have shown significant impacts on all types of business in both developed and developing countries. Both direct and indirect impacts of natural disasters are devastating to business activities and their continuity. These catastrophic events have created a significant negative impact on most of the business entities during recent years [1]. In addition, according to the latest findings of the nonprofit German Observatory, nearly half a million people have died from diseases related to climate disasters in the past two decades the past 20 years.

In late March 2021, people living on the east coast of Australia experienced a rare meteorological event. Record-breaking rainfall in some areas and very heavy and sustained rainfall in others led to severe flooding. However, in different places, the disaster was described as a once-in-thirty-year, once-in-five-year, or once-in-100-year event. For meteorologists, every 100 years means that one or more events occur every 100 years on average. The exact probability still varies

from place to place. In parts of the United States, events that occur more than once in 100 years are more frequent than events that occur once in a century.

In this paper, we determine the frequency of weather events based on the average return period. The average return period is the reciprocal of the probability of occurrence per year. For an event with an annual probability of 0.01, the average return period is 100 years, i.e., the once-in-100-year event mentioned in the data, i.e., a once-in-100-year event is not the same as an event that occurs once or at least once every 100 years.

Weather events are mainly expressed by the three aspects of damage degree, damage extent, and duration of weather events. Damage extent refers to the damage to people and property brought about by disasters like typhoons, rainstorms, and earthquakes in a nonman-made force majeure [2]. The extent of damage refers to the extent of damage impact brought about by natural disasters in the spatial dimension, for people and property. Weather event duration refers to the duration of the weather event in days [3].

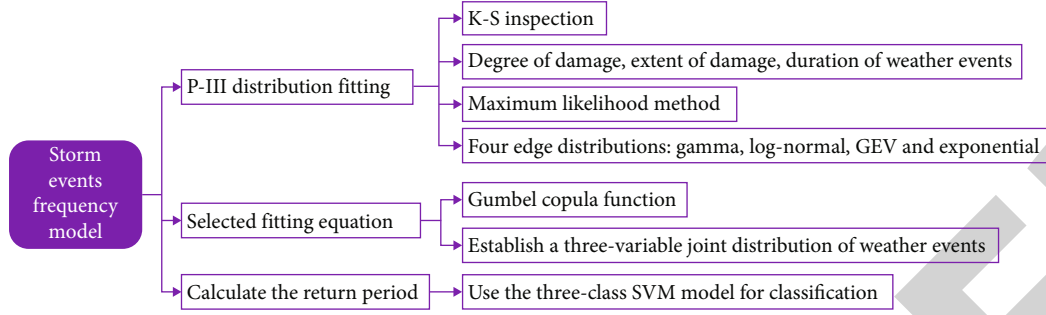


FIGURE 1: The idea of the storm event frequency model.

In the study of weather events, early scholars focused on the impact of disasters [4, 5] and later extended to regional and economic studies [6–8]. Ordinary least squares (OLS) can only estimate the parameters in a global or average sense and cannot reflect the spatial local variability; so, it cannot reveal the spatial dependence; geographically weighted regression (GWR) can estimate each parameter spatially and can better reflect the spatial dependence among the factors affecting the occurrence of extreme weather events.

In this paper, we established a weather event frequency analysis model, analyzed the return period of weather events, and considering the spatial heterogeneity in the country, such as the latitude and longitude of each state, natural environment, and social environment, and a geographically weighted regression model is established to deduce the temporal and spatial pattern of weather time development in the United States and predict the relative frequency of weather events in different regions. The research method in this paper is well generalized and innovative in the frequency prediction of extreme events.

2. Basic Assumptions

To simplify the problem, we make the following basic assumptions. (i) We define that all research objects are randomly distributed in space. In Moran index analysis, we can calculate the index value by placing the observation index in the same space state through this assumption. (ii) All observation indicators are not independent in space, and the spatial relationship is nonstationary. For the spatial geographic weighted regression model, because of the correlation between the indicators, different spaces are heterogeneous and nonstationary and thus have different effects on the observation indicators. (iii) The observation index of each unit can be seen as a point in space. (iv) For spectral clustering analysis, because points in different areas of space constitute a point set, therefore, we can use distance to measure the degree of spatial correlation.

3. Storm Event Frequency Model Based on Copula

3.1. Concept Introduction. There is a certain relationship between the intensity of a natural event and its probability of occurrence, as discussed elsewhere [9]. The greater the

intensity, the less likely or the lower the probability of occurrence, such as the rare Australian meteorological event in March mentioned in the data, which caused a very serious flood. Such events are called low-probability events and are usually obtained by extrapolation of extreme distribution functions, but the error range becomes larger as the degree of extrapolation expands. In addition, the results obtained by using different distribution functions are not the same. We assume that the probability of occurrence of such an event is P , and the time interval between its reoccurrence and the initial time is T ; we call it the average return period, which can be expressed as follows:

$$\begin{cases} T = \sum_{n=1}^{\infty} np(n), \\ p(n) = p(1-p)^{n-1}. \end{cases} \quad (1)$$

Among them, n is the return period, $p(n)$ is the probability that the return period is n , and the average return period can be obtained from the above formula. That is, the average return period $T = 1/p$ is the inverse of the annual probability of occurrence, as discussed elsewhere.

For example, for an event with an annual probability of 0.01, the average return period is 100 years, that is, the once-in-100-year event mentioned in the data; that is, the once-in-a-hundred-year event is not equal to an event that will occur once or at least once in 100 years [10]. However, a once-in-a-hundred-year event does not mean an event that will occur once or at least once in 100 years. The probability of such a small event needs to be extrapolated from the extreme distribution function; that is, the lower the probability of occurrence, the greater the intensity of the event. Based on this idea, we build a frequency analysis model which is shown in Figure 1.

3.2. Weather Event Frequency Model Based on Copula Function. To construct a multivariate copula function, it is necessary to determine the marginal distribution function of the variable. Based on the domestic and foreign research on the marginal distribution of flood events in various weather events [11–14], this paper first adopts the P-III distribution for fitting calculation. To further improve the fitting accuracy and select the best fitting function, this paper selects four marginal distributions of gamma, log-normal, GEV, and exponential to fit the damage degree (S), damage

range (D), and weather event duration (T) sequence [15]. First, the maximum likelihood method is used to estimate the marginal distribution parameters, and the K - S test method is used to verify the fit.

The Kendall rank correlation coefficient is used to describe the correlation degree of different variables [16, 17]. The calculation formula is as follows:

In the formula, n is the length of the weather event sequence, sign is the sign function, and $\{(x_1, y_1) \cdots (x_n, y_n)\}$ is the random sample in the data event.

3.3. Construction of Joint Distribution of Weather Event Variables. Copula function is a multivariate function subject to uniform distribution, and its domain is $[0,1]$. By supposing F_1, F_2, \dots, F_n is a continuous random variable, then there is a unique Copula function C which is generated that satisfies the formula for any $X \in R$:

$$F(x_1, x_2, \dots, x_n) = P\{X_1 \leq x_1, X_2 \leq x_2, \dots, X_n \leq x_n\} = C[F_1(x_1), F_2(x_2), \dots, F_n(x_n)], \quad (2)$$

where x_1, x_2, \dots, x_n is a different sample, and $F(x)$ is a marginal distribution function.

Based on the data characteristics of weather events from 2001 to 2021, this paper summarizes and extracts three one-dimensional index data, namely, the degree of damage, the extent of damage, and the duration of the weather event. These three levels of indicators can more fully reflect the characteristics of any weather event in the data, and the joint distribution function is selected based on this characteristic data. In this article, two elliptical copula functions (t and Gaussian) and three symmetrical Archimedean functions are used to construct the two-dimensional joint distribution of damage degree-damage range, damage degree-weather event duration, and damage range-weather event duration and adopt two kinds of symmetry, and three asymmetric distributions are used to build the three-dimensional joint distribution of damage degree-damage range-weather events; the maximum likelihood method is used to estimate parameters; root means square error R_{RMSE} criterion and A_{AIC} information criterion method are used to judge the goodness of fit. The smaller the value, the higher the degree of fit [18]. The calculation formula is follows:

$$\begin{cases} M_{\text{MSE}} = \frac{1}{n} \sum_{i=1}^n (p_{ei} - p_i)^2, \\ A_{\text{AIC}} = n \ln(M_{\text{MSE}}) + 2k, \\ R_{\text{RMSE}} = \sqrt{M_{\text{MSE}}}. \end{cases} \quad (3)$$

In the formula, n is the weather event sequence length, k is the number of Copula parameters, i is the sequence number in descending order, p_i is the theoretical value of the i -th joint distribution, p_i is the i -th empirical value, and M_{MSE} is the mean square error.

3.4. Return Period Calculation. The calculation formula of the univariate return period T is $T = 1/[1 - F(x)]$. In the for-

mula, $F(x)$ is the univariate marginal distribution function. The calculation formula for the joint return period $T_a(x, y)$ and the co-occurrence return period $T_b(x, y)$ of the two variables X and Y is as follows:

$$\begin{cases} T_a(x, y) = \frac{1}{1 - F(x, y)} = \frac{1}{1 - C(u, v)}, \\ T_b(x, y) = \frac{1}{1 - u - v + c(u, v)}. \end{cases} \quad (4)$$

Among them, U and V are marginal distribution functions; $C(u, v)$ is the two-variable joint distribution function.

The calculation formula for the joint return period $T_a(x, y, z)$ and the co-occurrence return period $T_b(x, y, z)$ of the three variables x, y and z is as follows:

$$\begin{cases} T_a(x, y, z) = \frac{1}{1 - C(u, v, w)}, \\ T_b(x, y, z) = [1 - u - v - w + C(u, v) + C(u, w) + C(v, w) - C(u, v, w)]^{-1}. \end{cases} \quad (5)$$

Among them, u, v, w is the marginal distribution function; $C(u, v), C(u, w), C(v, w)$, is the two-variable joint distribution function; $C(u, v, w)$ is the three-variable joint distribution function.

3.5. Model Construction. The fitting test and correlation coefficient of the marginal distribution function of each univariate damage degree (S), damage scope (D), and weather event duration (T) are shown in the following table. Table 1 shows that the characteristic variables of weather events are more correlated well, the degree of damage has the strongest correlation with the duration of the weather event, $\varphi = 0.6239$, followed by the degree of damage and the scope of the damage, $\varphi = 0.6007$, and the degree of damage has the weakest correlation with the duration of the weather event, $\varphi = 0.5981$.

At the confidence level $\alpha = 0.05$, the statistic value of each variable K is less than the critical value; so, the K - S test is accepted. The higher the ρ value and the lower the k statistic value, the distribution function is selected as the univariate marginal distribution function of the weather event in the data, that is, the degree of weather event damage. The sequence selects the gamma distribution, the weather event range selects the log-normal distribution, and the weather event duration selects the P -III type distribution. The parameter values are shown in Table 1.

3.6. The Establishment of the Optimal Copula Function. The two-variable and three-variable joint distribution fitting test and parameter values are shown in Table 2. Table shows the best fitting function of the two-variable and three-variable joint distribution. As can be seen from Table 2, the Gumbel Copula function is the best fit for the joint release of the three variables. The fitting effect of the joint distribution of variables is the best. Therefore, Gumbel copula is used to analyze the three-variable return period of damage degree (S), damage scope (D), and weather event duration (T).

TABLE 1: Test statistics and correlation coefficient of marginal distribution function.

Variable	Fitting function	p	Statistic value k	Critical value d	Correlation coefficient r
Extent of damage	Gamma	0.8701	0.1821	0.3226	S-D (0.6007)
	Log-normal	0.7557	0.1524	—	—
	GEV	0.1265	0.2849	—	—
	exp	0.2782	0.2523	—	—
	P3	0.7249	0.1049	—	—
Damage scope	Gamma	0.4721	0.3426	0.3226	S-T (0.6239)
	Log-normal	0.7932	0.2576	—	—
	GEV	0.3425	0.1027	—	—
	exp	0.4192	0.4026	—	—
	P3	0.2491	0.2849	—	—
Weather event duration	Gamma	0.8047	0.1239	0.3226	D-T (0.5981)
	Log-normal	0.8245	0.1597	—	—
	GEV	0.9042	0.9034	—	—
	exp	0.8201	0.1942	—	—
	P3	0.9625	0.0892	—	—

*Note: the boldface in the table is the optimal marginal distribution function.

TABLE 2: Three-variable joint distribution of weather events.

Function type	Parameter	R_{RMSE}	A_{AIC}
Clayton	2.74	0.062	-40.7
Frank	7.52	0.051	-52.4
Gumbel	2.42	0.046	-51.9
Joe	2.97	0.069	42.5
NC	4.420/4.252	0.057	-49.2
NJ	3.024/2.563	0.049	-42.5

TABLE 3: Weather event return period.

Weather event type	Return period	Weather event type	Return period
Thunderstorm wind	30	Ice storm	50
Flash flood	30	Wildfire	50
Winter weather	30	Extreme cold	50
High wind	30	Coastal flood	50
Marine hail	100	Seiche	100
Marine tropical depression	100	Sneaker wave	100

3.7. *Model Results.* Establish the three-variable joint distribution of weather events based on the selected Gumbel Copula function, calculate the joint and co-occurrence return periods, and calculate the three-variable joint distribution return periods under different univariate returns periods [19, 20]. The results are shown in Table 3.

We further classify the return periods of weather events in the data through the three-class SVM model, and the results are shown in Figure 2.

4. Spatial Correlation Analysis: Moran Index

To further study the features of extreme weather events, we analyze the spatial regularity of several weather events using the Moran index and geographically weighted regression models [21].

Moran index is divided into global Moran index and local Moran index, which are used to judge the degree of aggregation and dispersion of the index in the global and local, respectively.

Moran I (global Moran index) is defined as follows:

$$\text{MoranI} = \frac{\sum_{i=1}^n w_{ij}(y_i - \bar{y})(y_j - \bar{y})}{s^2 \sum_{i=1}^n w_{ij}}. \quad (6)$$

In it,

$$s^2 = \frac{1}{n} (y_j - \bar{y}), \bar{y} = \frac{1}{n} \sum_{i=1}^n y_i. \quad (7)$$

\bar{y} is the selected index value of the place (observation value), n is the total number of units in the whole area, and w_{ij} is the binary adjacent space weight matrix; according to whether the two units are adjacent or not, the value of w_{ij} is

$$w = \begin{bmatrix} w_{11} & \cdots & w_{1n} \\ \vdots & \ddots & \vdots \\ w_{n1} & \cdots & w_{nn} \end{bmatrix}. \quad (8)$$

$$w_{ij} = \begin{cases} 1 (i \text{ is adjacent to } j) \\ 0 (i \text{ is not adjacent to } j) \end{cases},$$

$$i = 1, 2, \dots, 48, j = 1, 2, \dots, 48 (i \neq j).$$

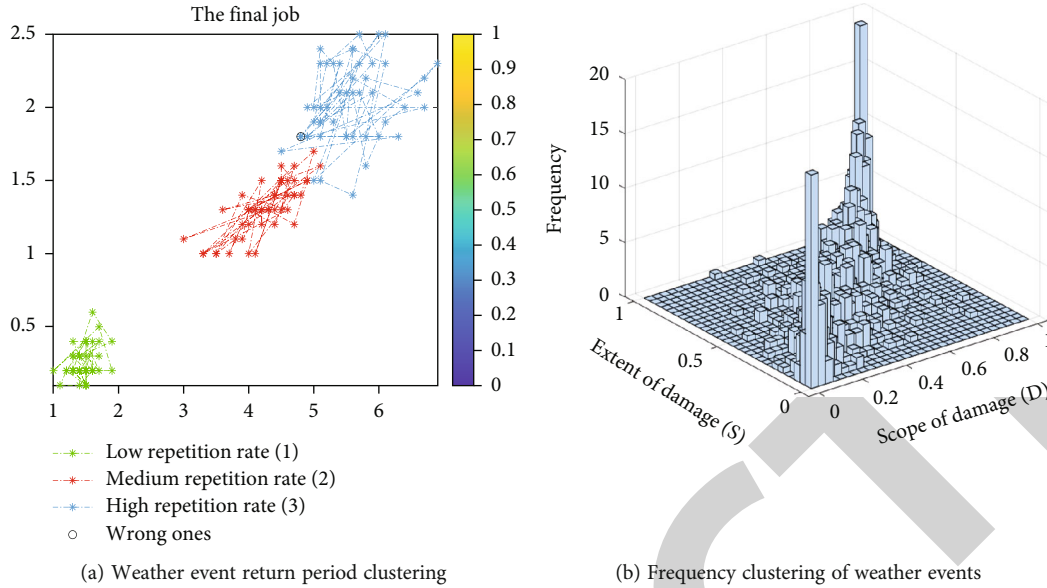


FIGURE 2: Weather event clustering.

Moran I is the product sum of observations in various regions, and its value range is in $[-1, 1]$ [22].

Moran

$$I \begin{cases} >0 (\text{The larger the value, the more significant the aggregation benefit}), \\ =0 (\text{No spatial correlation}), \\ <0 (\text{The smaller the value, the more significant the discrete benefit}). \end{cases} \quad (9)$$

It needs to be tested for the H_0 hypothesis, the hypothesis test that all the research objects are randomly distributed in the space. Next, the Z test is used for verification.

$$Z = \frac{I - E(I)}{\sqrt{\text{var}(I)}}. \quad (10)$$

In it, the calculation formula of $E(I)$ and $\text{Var}(I)$ is as follows:

$$E(I) = -\frac{1}{n-1},$$

$$\text{Var}(I) = \frac{n^2(n-1)1/2\sum_{i \neq j} (w_{ij} + w_{ji})^2 - n(n-1)\sum_{i=1}^n (w_{kj} + w_{jk})^2 - 2(\sum_{i \neq j} w_{ij})^2}{(n+1)(n-1)^2\sum_{i \neq j} w_{ij}(\sum_{i \neq j} w_{ij})}. \quad (11)$$

Under the standard of significance of 0.05, as long as $|z| > 1.96$ or $(p < 0.05)$, the H_0 null hypotheses can be rejected, and all research objects are randomly distributed in space [22].

We calculated the global Moran index for the six weather events, and the results are shown in Figure 3. The abscissa represents the described variable, and the ordinate represents the spatial lag vector of the described variable. The four quadrants correspond to the four spatial aggregation effects

of high-high clustering, low-high clustering, low-low clustering, and high-low clustering. Figure 4 corresponds to the permutation test results of each variable Moran index and the corresponding statistics.

According to the p value of the global Moran index, among the six weather events, thunderstorm wind, flash flood, extreme cold/wind chill, and dense fog have significant spatial aggregation effects; blizzard and frost/freeze have lower spatial aggregation effects.

5. Spatial Law Exploration: GWR Model

The geographical weighting model (GWR model) is a model for spatial nonstationarity caused by changes in the relationship or structure of variables caused by changes in geographic location [23–25].

Here are the stats for weather events and latitude and longitude by state.

The general form of the model is as follows:

$$y_{\{i\}} = \beta_0(i) + \beta_1(i)x_{1,\{i\}} + \beta_2(i)x_{2,\{i\}} + \dots + \beta_k(i)x_{k,\{i\}} + \mu_{\{i\}}. \quad (12)$$

Among them, (i) represents the region, and $\{i\}$ represents the sample set included in the estimation; here, we select 48 states in the United States.

According to the principle of borrowing points, each local point obtains data from the surrounding area to form a different sample set for each region. Here are the stats for weather events and latitude and longitude by state. Establishing a new spatial weight matrix is as follows.

$$A_{\text{ICC}} = 2n \ln(\sigma) + n \ln(2\pi) + n \left(\frac{n + \text{tr}(s)}{n - 2 - \text{tr}(s)} \right). \quad (13)$$

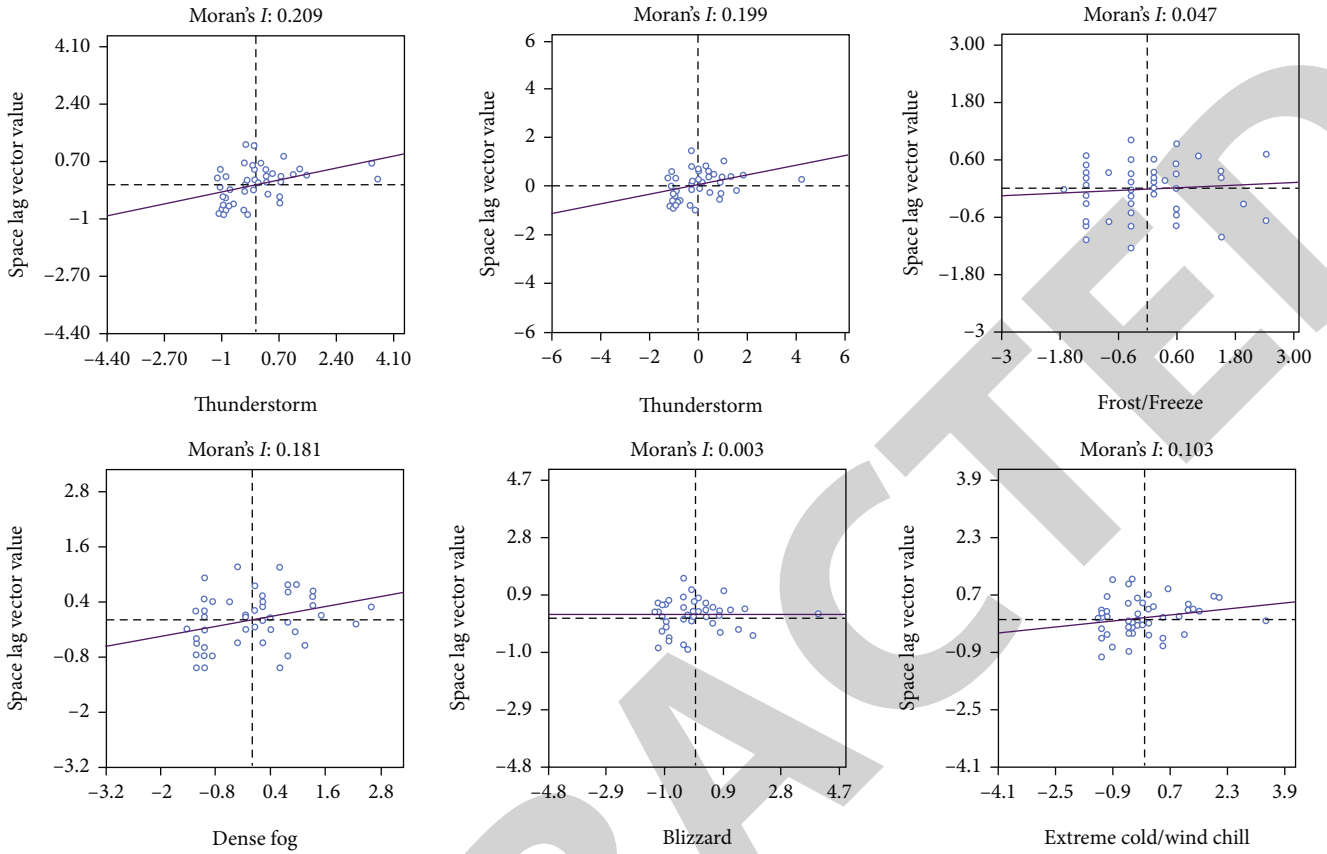


FIGURE 3: Global Moran index results for six types of weather.

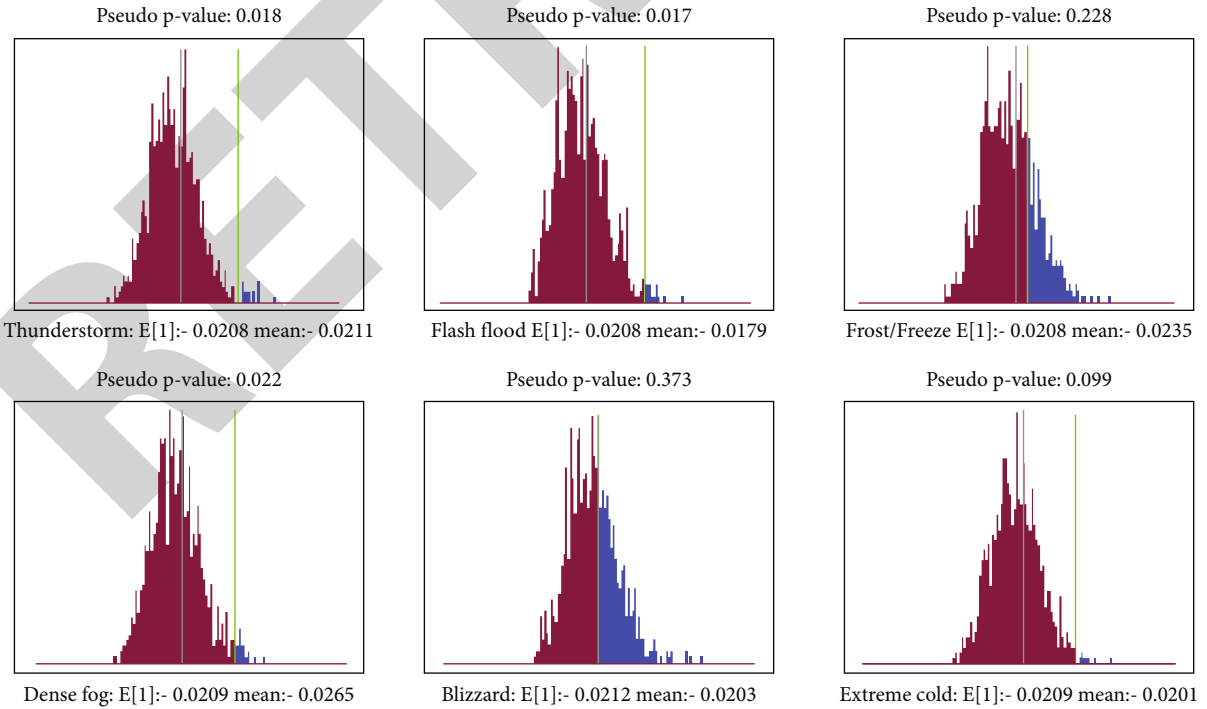


FIGURE 4: Test result of global Moran index after permutations.

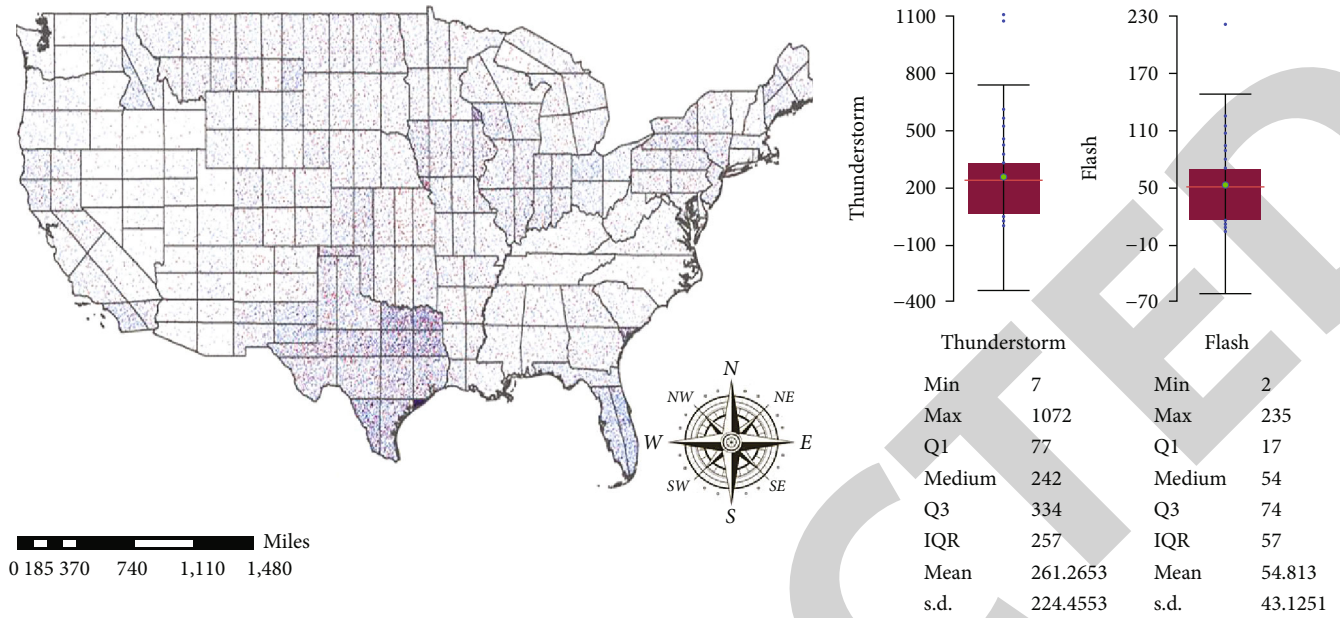


FIGURE 5: Thunderstorm wind and flash flood event correlation diagram.

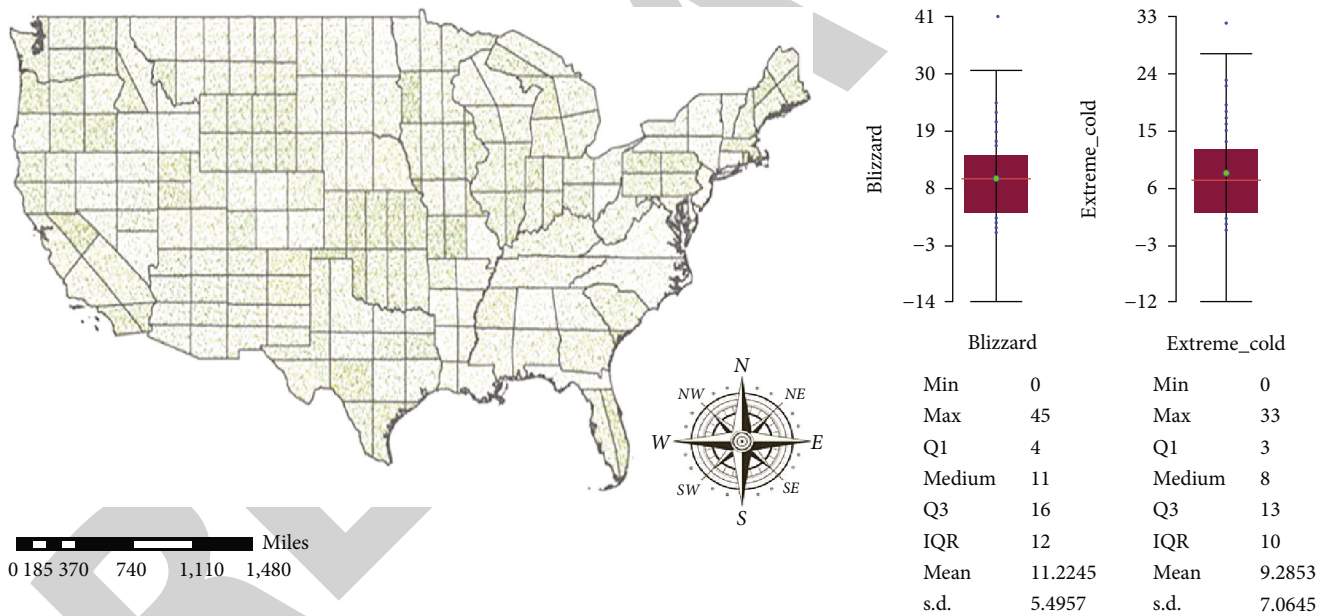


FIGURE 6: Blizzard and extreme cold/wind chill event correlation diagram.

The value of A_{ICC} is determined by the number of independent parameters and the maximum likelihood function of the model.

We count the relevant data of 2005, 2010, 2015, and 2020 to establish a geographically weighted regression model. The model results are shown in Figures 5–7.

Table 4 shows the model test results reflect that the GWR model exhibits larger goodness of fit R^2 , a smaller AICC value, residual sum of squares, and residual estimated standard deviation sigma value. Based on the results of the GWR model, the following conclusions were found.

Thunderstorm wind and flash flood have the highest frequency in the United States, showing a spatial trend of increasing from west to east and from north to south. Extreme cold/wind chill and blizzard occur in the middle frequency, and the frequency of extreme cold/wind chill on the west coast is much lower than that of the central and east coasts. The frequency of blizzard in the western states of California, Nevada, Arizona, and Iowa is much lower than the frequency in the central and eastern states. Dense fog and frost/freeze have a relatively stable distribution throughout the United States. Except for the four states on the east coast of New Jersey, Connecticut, Vermont,

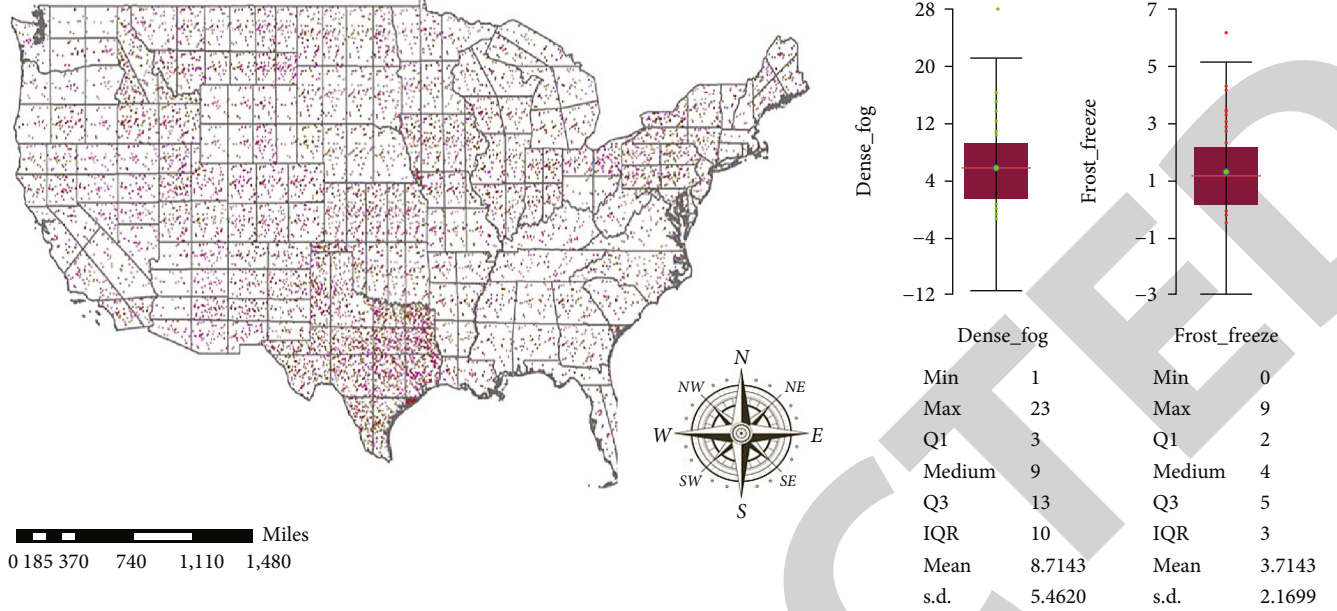


FIGURE 7: Dense fog and frost/freeze event correlation diagram.

TABLE 4: Geographically weighted regression model test results.

R^2	-2log-likelihood	A_{ICC}	Residual squares
0.8221	0.8491	0.9021	0.8743
-192.43	-187.65	-74.63	-117.65
-138.12	-137.82	-30.41	-42.84
762.84	692.29	721.62	965.62

and Maryland, where the frequency is higher, and the frequency of Texas is lower, the other states as a whole presents a relatively stable probability of occurrence.

Here, we divide the United States into five regions and perform descriptive statistics on the data to help illustrate the existence of certain spatial patterns in weather events. We select two typical weather events: flash floods and tornadoes and count their occurrences from 2010 to 2020, which is shown in Figure 8.

From the results of the descriptive statistics, it can be seen that the number of weather events changes with the time series, and the changing trends of regional weather events are different. In recent years, the frequency of flood disasters has increased in the east coast region, while the frequency in the central region has been almost unchanged. In contrast, tornado disasters have shown a relatively stable frequency of occurrence in recent years. Here, we should also note that different weather events are likely to show different spatial and temporal patterns in different regions and even globally, and not all-weather events are affected by climate change and become frequent.

6. Prediction of Frequency of Extreme Weather Events

6.1. Research Ideas. For this weather event, this article first uses an improved wavelet neural network model to predict

the total probability of the occurrence of various extreme weather events from 2010 to 2020. Perform this intelligent algorithm to replace the neurons in the traditional artificial neural network with wavelet elements based on wavelet analysis. Through mathematical transformation, the weights from the input layer to the hidden layer are transformed into new expansion parameters and the critical value of the hidden layer [26–29].

6.2. Research Method. The activation function of the hidden layer in the network diagram can be expressed as

$$g_j(x) = \prod_{i=1}^p \Psi \left(\frac{x_i - b_{ij}}{a_{ij}} \right). \quad (14)$$

Among them, Ψ represents the corresponding wavelet operation, X is the network input, i represents the different input wavelet elements in the network, and j is the network middle layer code and represents the new expansion and translation parameters after transformation. Therefore, the output function of the wavelet neural network can be expressed as

$$f_i(x) = \sum_{j=1}^h \omega_{ij} g_j(x). \quad (15)$$

In the formula, h is the number of levels of the wavelet network, and ω_{ij} is the output weight.

Although the functions and parameters of the traditional wavelet neural network are obtained after wavelet transformation, the transformation method is single and fixed, which cannot adapt to the complex and changeable conditions of weather events. At the same time, it is easy to cause

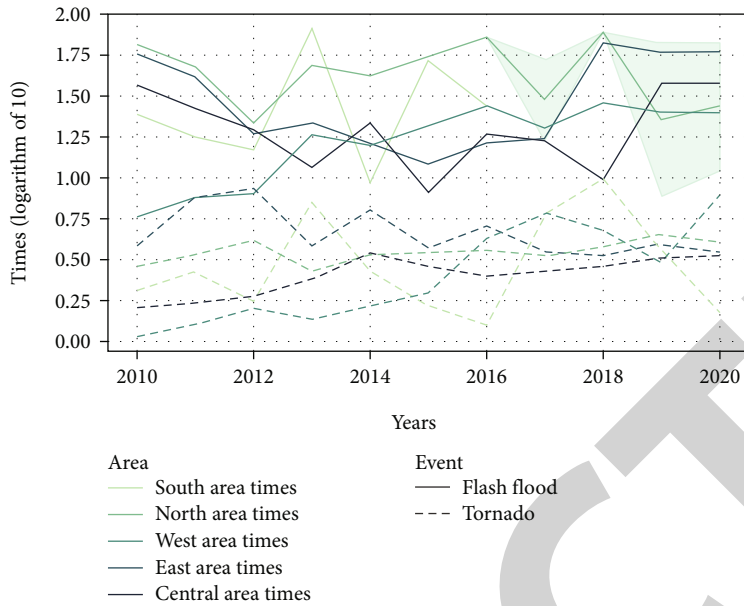


FIGURE 8: Frequency map of weather events in different regions over time.

the algorithm to reduce the approximation rate. Make random improvements:

To solve the problem of approximation rate, the improved excitation function and output function are, respectively,

$$\begin{cases} g'_j(x) = \prod_{i=1}^p \Psi, \left(\frac{\sum_{k=1}^n \omega_{jk} x_k(t) - b_j}{a_j} \right), \\ f'_i(x) = \sum_{j=1}^N \omega_{ij} \prod_{i=1}^p \Psi \left(\frac{\sum_{k=1}^n \omega_{jk} x_k(t) - b_j}{a_j} \right). \end{cases} \quad (16)$$

In the above formula, k represents the output layer code, N is the total number of wavelet elements, and p is the number of training sample spaces. According to the numerical characteristics, the expression of the error function can be obtained as

$$E = \frac{1}{2} \sum_{p=1}^P \sum_{i=1}^N (d_i^p - y_i^p)^2. \quad (17)$$

In the above formula, d represents the mathematical expectation of the output layer, and y_i represents the actual network output value.

6.3. Result Analysis

Step 1. Determination of input and output. Through the descriptive analysis of the factors affecting the occurrence of extreme weather events, it is found that the frequency of extreme weather events was as follows.

Affected by precipitation factors, climatic factors, and personnel activity factors, it has a certain degree of randomness.

Therefore, the above three parameters are used as the input of the random wavelet network extreme weather event prediction model. In order to simplify the model, the year is the smallest unit, and the once-in-a-hundred-year event obtained in the first question is regarded as the most destructive weather event, that is, the extreme weather event. The ratio of the number of extreme weather events in the Americas to the number of all-weather events is taken as the probability of extreme weather events, and this probability is taken as the output of the random wavelet network extreme weather event probability prediction model.

Step 2. Hidden layer unit determination. In wavelet neural networks, the choice of the number of hidden layer units is also critical. The number of hidden units is too small, and the entire network cannot be well [30].

Information processing is as follows: too many hidden units will directly lead to structural redundancy and fall into local minimums. To balance the relationship between the two, the following formula is usually used to determine the number of hidden units of the wavelet neural network.

$$Z = \sqrt{mn + 1.68n + 0.93}. \quad (18)$$

Among them, Z is the number of hidden layer units, n is the number of network inputs, and m is the number of network outputs. Combining the number of inputs and outputs of the extreme weather event prediction model, substituting $n = 3$ and $m = 1$, $z = 2.99$ can be obtained. Therefore, the number of hidden layer units of the foundation pit settlement prediction model based on random wavelet network is set 3 which is appropriate.

This article uses MATLAB software to check the fitting and prediction results of the wavelet neural network model

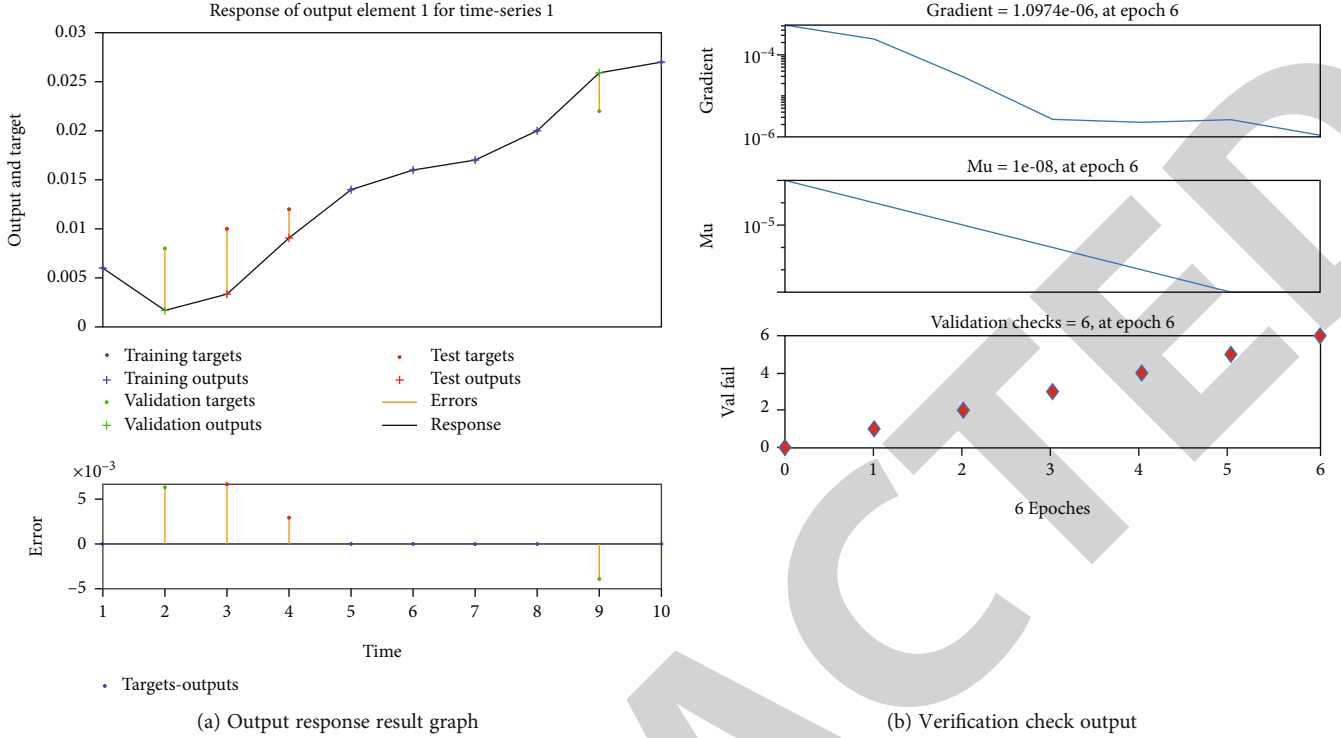


FIGURE 9: Model result graph.

[31–33]. The results can be seen in Figure 9. It can be seen from the results of validation checks that with the training of the network, the error of the confirmation sample has basically no longer been reduced, and it has been 4 times in a row. In the iteration, the error curve no longer drops, and the condition for the termination of training is generated at this time. From the fitting prediction results of the wavelet neural network model on the probability of extreme weather events, it can be concluded that the total probability of extreme weather events in the past ten years has shown a roughly rising trend, and from the predicted value, it is known that there is a high probability of extreme weather events in 2021. The probability of weather occurring in the entire Americas can reach around 0.016. The reason is that as forests and other vegetation have been destroyed on a large scale, the population has increased rapidly and is caused by global warming. Global warming means that the evaporation of water on the earth's surface increases, and a large amount of water vapor melts into the air, forming raindrops, rainstorms, and floods, and the temperature of the ground is getting higher and higher, which leads to droughts and sandstorms in some areas. The frequency and intensity of disasters such as droughts and floods will also increase. A wide range of extreme weather and climate events have severely affected life and production.

7. Evaluation and Spread of the Model

Although we analyzed the spatial laws of national weather events based on considering spatial heterogeneity, we still need to improve the model accuracy and outliers due to the shortcomings of the GWR model itself. For the accuracy

of the model, we should modify the fixed bandwidth in the model by using smaller bandwidths in regions with dense data points and larger bandwidths in regions with data point coefficients and by adding Bayesian information to the model measurements. Thus, the accuracy of the model will be further improved [34–36]. For outliers in the results, we should add the local Moran index, compare the global and local Moran index results, and eliminate outliers. The flow of the model improvement is shown in Figure 10.

In the process of using Bayesian inference methods to deal with sudden changes in extreme weather events, it is first necessary to calculate its posterior expectation with the following equation.

$$E(a|h) = \int_{\theta} a \cdot \theta \cdot P(\theta|h) d\theta, \quad (19)$$

where a is any distribution function assuming a model containing θ parameters, θ is the model parameters, and $E(a|h)$ is the posterior expectation of extreme events. The MCMC algorithm is used to carry out the solution problem of integration. The MCMC algorithm is also known as the Monte Carlo simulation algorithm of Markov chain. The formula of this algorithm is as follows.

$$E(a|h) \approx \frac{1}{N} \sum_{i=1}^N a(\theta^{(i)}). \quad (20)$$

In the formula, $\theta^{(1)}, \theta^{(2)}, \dots, \theta^{(N)}$, is the mean of a sample from a simulated Markov chain that obeys a priori

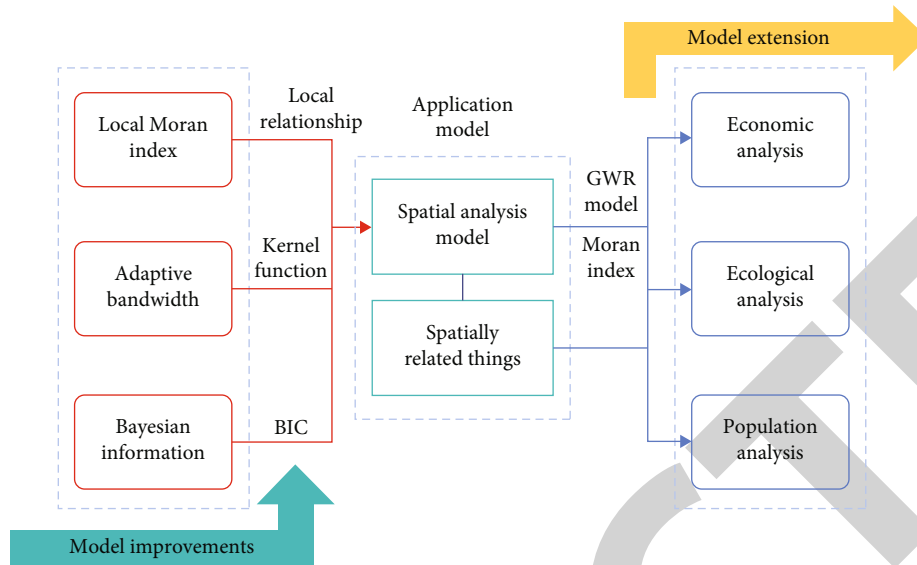


FIGURE 10: Model improvements and extensions.

probability distribution of $P(\theta|h)$ and whose value is an unbiased estimate.

The calculation of the complete reversible jump Markov Monte Carlo method BJM-CMC algorithm needs to be done by the following steps. First, the jump probability matrix between different model assumptions is determined $J(H_k \rightarrow H_{k'})$ and sampled from the simulated distribution of weather events $Q(u_k|H_k, H_{k'})$ to obtain u_k . Next, we set the transformation matrix $Q_{k'}, u_{k'} = g_{k,k'} \theta_k u_k$. Calculate the concession ratio m from H_k to $H_{k'}$. The probability that $H_{k'}$ is better than H_k is defined as him_1 , m . If $him_1, m = 1$ then the jump to $H_{k'}$ is rejected. If $him, m < 1$, then reject H_k and retain the original hypothesis $H_{k'}$, where the expression for m is as follows:

$$m = \frac{P(h|\theta_{k'}, H_{k'})P(\theta_{k'}|H_{k'})P(H_{k'})J(H_{k'} \rightarrow H_k)Q(u_k|\theta_{k'}, H_{k'}, H_k) \left| \frac{\partial g_{k,k'} \theta_k, u_k}{\partial (\theta_k, u_k)} \right|}{P(h|\theta_k, H_k)P(\theta_k|H_k)P(H_k)J(H_k \rightarrow H_{k'})Q(u_k|\theta_k, H_k, H_{k'})} \quad (21)$$

The spatial model of this paper, in addition to statistics and prediction of the spatial laws of weather events in the country, can also predict the property losses, casualties, and so on indirectly caused by disasters. If we need to make the statistical results more accurate, we can choose a smaller spatial unit, such as selecting counties as the basic spatial units, then we can analyze the spatial regularity of weather events in a certain region or state. Further, we can change the research object and choose all things that may have spatial laws, such as economy, ecology, and population, and analyzing the spatial laws of such things will be of great significance to the scientific development of society [33].

8. Conclusion

To build a weather event frequency analysis model. In this paper, four edge distributions of gamma, log-normal, GEV, and exponential are selected for fitting, and it is concluded that

the Gumbel Copula has the best fitting effect. Second, the maximum likelihood method was used to estimate the marginal distribution parameters, and the K -S test method was used to verify the fit. Then, based on the selected Gumbel Copula function, the three-variable joint distribution of weather events is established, and the joint co-occurrence regression period and the three-variable joint distribution regression period under different univariate regression periods are calculated, respectively. Finally, the SVM model is used to classify the obtained results to better present the data features.

The combination of the Moran index and the geographically weighted regression model used in this article can well predict the indicators and data with spatial distribution characteristics under the premise of considering spatial heterogeneity and nonstationarity. Studies have found that the United States has the highest frequency of thunderstorms and flash floods, showing a spatial trend of increasing from west to east and from north to south. Finally, through the establishment of an ARIMA model to predict the frequency of weather events, it is found that the total number of thunderstorms is on the rise. It can be seen that as the years go by, thunderstorms have become more frequent. Torrent data is close to stable. The frequency of blizzards, dense fog, and frost/icing has generally increased.

Then, a wavelet neural network model is established to predict the probability of extreme weather events across the Americas. It is concluded that the total probability of extreme weather events in the past ten years shows a roughly rising trend, and from the predicted value, it can be known that by 2021, the probability of extreme weather events in the entire Americas can reach around 0.016.

Data Availability

Data for this paper were obtained from the National Oceanic and Atmospheric Administration's SPC report and NOAA's National Weather Service input for the period January 1950 to October 2021.

Conflicts of Interest

The authors declare that there are no conflicts of interest regarding the publication of this paper.

Authors' Contributions

Peng-Hui Yang contributed to the methodology, conceptualization, supervision, and leadership. Yao Yu contributed to the conceptualization, visualization, software, validation, and writing manuscript. Feng Gu contributed to the data collation, visualization, verification, and investigation. Meng-Jie Qu contributed to the software, method design, validation, and data analysis. Jia-Ming Zhu contributed to the verification, supervision, and writing review and editing. All authors read and approved the final manuscript.

Acknowledgments

This study was funded by the National Social Science Fund Project of China (21CTJ024), the Teaching and Research Fund Project of the Anhui University of Finance and Economics (acxkjs2021005 and acyljc2021002), Anhui Quality Engineering Project Teaching Demonstration Course “mathematical modeling” (2020SJJXSF0018), and Provincial Online and Offline First-Class Course “Advanced Algebra” (2020xsxxkc018).

References

- [1] G. Samantha, “The impact of natural disasters on micro, small and medium enterprises (MSMEs): a case study on 2016 flood event in Western Sri Lanka,” *Procedia Engineering*, vol. 212, pp. 744–751, 2018.
- [2] J. Fang and P. Shi, “A review of coastal flood risk research under global climate change,” *Progress in Geography*, vol. 38, no. 5, pp. 625–636, 2019.
- [3] N. Bhattacharya, J. Elizabeth, D. Proverbs, and F. Hammond, “Development of conceptual framework for understanding vulnerability of commercial property values towards flooding,” *International Journal of Disaster Resilience in the Built Environment*, vol. 4, no. 3, pp. 334–351, 2013.
- [4] Z. Chi, M. Jaboyedoff, M.-H. Derron, and C. J. Van, “An interactive web-GIS tool for risk analysis: a case study in the Fella River basin, Italy,” *Natural Hazards and Earth System Sciences Discussions*, vol. 16, no. 1, pp. 85–101, 2016.
- [5] M. Haggag, A. Siam, W. El-Dakhkhni, P. Counlibaly, and E. Hassini, “A deep learning model for predicting climate-induced disasters,” *Natural Hazards*, vol. 107, no. 1, pp. 1009–1034, 2021.
- [6] Z. Zhang, C. Gao, Q. Liu et al., “Risk assessment of rainstorm and flood disasters in the Huaihe River basin in different recurrence periods,” *Geographical Research*, vol. 33, no. 7, pp. 1361–1372, 2014.
- [7] G. F. Zhang, X. C. Zha, and G. P. Wang, “Risk assessment of flood disasters in different return periods along the Ankang reach of the Hanjiang River,” *Journal of Lanzhou University (Natural Sciences)*, vol. 55, no. 5, pp. 571–577, 2019.
- [8] X. Yang and Q. Liu, “Forecast of economic loss from storm surge disaster based on KPCA-RBF model,” *Marine Sciences*, vol. 45, no. 10, pp. 32–39, 2021.
- [9] Y. Li and R. Hu, “Research on Heilongjiang Province heavy rain event disaster assessment and pre-evaluation model based on grey correlation,” *Journal of Catastrophe*, vol. 31, no. 2, pp. 78–83, 2016.
- [10] Y. H. Huang, Y. H. Zhu, Y. Hu, and X. L. Zhou, “Time series prediction based on wavelet analysis,” *Smart City*, vol. 7, no. 18, pp. 128–130, 2021.
- [11] M. Gui and L. Liu, “Prediction of the total retail sales of social consumer goods in Hainan Province based on the ARIMA model,” *Mathematics in Practice and Understanding*, vol. 47, no. 3, pp. 25–30, 2017.
- [12] G. Cheng, Y. Zhang, J. L. Huang, J. B. Liu, J. W. Zhang, and S. Zhang, “Vulnerability analysis of aqueduct structure based on boundary method,” *Earth and Environmental Science*, vol. 567, no. 1, article 012036, 2020.
- [13] P. Riley, B. Dan, Y. Liu, P. Verronen, H. Singer, and M. Güdel, “Extreme space weather events: from cradle to grave,” *The Scientific Foundation of Space Weather*, vol. 214, no. 1, pp. 7–9, 2018.
- [14] J. Huang, J. Jiang, J. Wang, and L. Hou, “Crop diversification in coping with extreme weather events in China,” *Journal of Integrative Agriculture*, vol. 13, no. 4, pp. 677–686, 2014.
- [15] P. Stott, N. Christidis, F. Otto et al., “Attribution of extreme weather and climate-related events,” *Climate Change*, vol. 7, no. 1, pp. 23–41, 2016.
- [16] N. S. Diffenbaugh, D. Singh, J. S. Mankin et al., “Quantifying the influence of global warming on unprecedented extreme climate events,” *Proceedings of the National Academy of Sciences of the United States of America*, vol. 114, no. 19, pp. 4881–4886, 2017.
- [17] M. D. Smith, “An ecological perspective on extreme climatic events: a synthetic definition and framework to guide future research,” *Journal of Ecology*, vol. 99, no. 3, pp. 656–663, 2011.
- [18] W. Cai, A. Santoso, G. Wang et al., “Increased frequency of extreme Indian Ocean Dipole events due to greenhouse warming,” *Nature*, vol. 510, no. 7504, pp. 254–258, 2014.
- [19] N. C. Duke, J. M. Kovacs, A. D. Griffiths et al., “Large-scale dieback of mangroves in Australia,” *Marine and Freshwater Research*, vol. 68, no. 10, pp. 1816–1829, 2017.
- [20] M. Trnka, R. P. Rötter, M. Ruiz-Ramos et al., “Adverse weather conditions for European wheat production will become more frequent with climate change,” *Nature Climate Change*, vol. 4, no. 7, pp. 637–643, 2014.
- [21] T. Oshan, Z. Li, W. Kang, L. J. Wolf, and A. Fotheringham, “MGWR: a Python implementation of multiscale geographically weighted regression for investigating process spatial heterogeneity and scale,” *International Journal of Geo-Information*, vol. 8, no. 6, pp. 269–300, 2019.
- [22] J. Tu, “Spatially varying relationships between land use and water quality across an urbanization gradient explored by geographically weighted regression,” *Applied Geography*, vol. 31, no. 1, pp. 376–392, 2011.
- [23] S. Li, C. Zhou, S. Wang, S. Gao, and Z. Liu, “Spatial heterogeneity in the determinants of urban form: an analysis of Chinese cities with a GWR approach,” *Sustainability*, vol. 11, no. 2, pp. 479–495, 2019.
- [24] A. F. Jan and H. Chan, “A wavelet neural network conjunction model for groundwater level forecasting,” *Journal of Hydrology*, vol. 407, no. 1–4, pp. 28–40, 2011.
- [25] A. Perera, V. M. Nik, D. Chen, J. L. Scartezzini, and T. Hong, “Quantifying the impacts of climate change and extreme climate events on energy systems,” *Nature Energy*, vol. 5, no. 2, pp. 150–159, 2020.

- [26] S. C. Van Pelt, J. J. Beersma, T. A. Buishand, B. J. Van den Hurk, and P. Kabat, "Future changes in extreme precipitation in the Rhine basin based on global and regional climate model simulations," *Hydrology and Earth System Sciences*, vol. 16, no. 12, pp. 4517–4530, 2012.
- [27] B. Pratt and H. Chang, "Effects of land cover, topography, and built structure on seasonal water quality at multiple spatial scales," *Journal of Hazardous Materials*, vol. 209-210, pp. 48–58, 2012.
- [28] Y. F. Zhou, H. E. Gang, L. Jin, and W. Wang, "Study on the coupling and coordination between economic development and ecological environment," *Journal of Anhui University of Science and Technology (Social science)*, vol. 20, no. 2, pp. 38–44, 2018.
- [29] J. M. Zhu, W. Y. Xia, J. J. Sun, J. B. Liu, and F. H. Yu, "The spread pattern on Ebola and the control schemes," *International Journal of Innovative Computing and Applications*, vol. 9, no. 2, pp. 77–89, 2018.
- [30] S.-M. Zhang, W.-L. Zhan, H. Hu, Y.-S. Liu, and J.-M. Zhu, "Research on ethanol coupling to prepare C4 olefins based on BP neural network and cluster analysis," *Journal of Chemistry*, vol. 2022, Article ID 5324336, 10 pages, 2022.
- [31] X.-W. Cai, Y.-Q. Bao, M.-F. Hu, J.-B. Liu, and J.-M. Zhu, "Simulation and prediction of fungal community evolution based on RBF neural network," *Computational and Mathematical Methods in Medicine*, vol. 2021, Article ID 7918192, 13 pages, 2021.
- [32] F. Xu, L.-Y. Mo, H. Chen, and J.-M. Zhu, "Genetic algorithm to optimize the design of high temperature protective clothing based on BP neural network," *Frontiers in Physics*, vol. 9, article 600564, p. 6, 2021.
- [33] Q. Z. He, P. T. Xia, B. Li, and J. B. Liu, "Evaluating investors' recognition abilities for risk and profit in online loan markets using nonlinear models and financial big data," *Journal of Function Spaces*, vol. 2021, Article ID 5178970, 15 pages, 2021.
- [34] J.-B. Liu, T. Zhang, Y. K. Wang, and W. S. Lin, "The Kirchhoff index and spanning trees of Mobius/cylinder octagonal chain," *Discrete Applied Mathematics*, vol. 307, pp. 22–31, 2022.
- [35] J.-B. Liu, Y. Bao, W. T. Zheng, and S. Hayat, "Network coherence analysis on a family of nested weighted n-polygon networks," *Fractals*, vol. 29, no. 8, article 2150259, p. 10, 2021.
- [36] J.-M. Zhu, Y.-G. Geng, W.-B. Li, X. Li, and Q.-Z. He, "Fuzzy decision-making analysis of quantitative stock selection in VR industry based on random forest model," *Journal of Function Spaces*, vol. 2022, Article ID 7556229, 12 pages, 2022.